A morphological-aggregative approach for 3D segmentation of pulmonary airways from generic MSCT acquisitions

Catalin Fetita[1], Margarete Ortner[1], Pierre-Yves Brillet[2], Françoise Prêteux[1], and Philippe Grenier[3]

1 Institut TELECOM / Telecom SudParis, Evry, France,
2 Université Paris 13, Avicenne Hospital, Bobigny, France,
3 Université Paris 6, Pitié-Salpêtrière Hospital, Paris, France

Abstract. Three-dimensional segmentation of airways from multi-slice computed tomography (MSCT) is a key point in the development of computer-aided tools for respiratory investigation. The expected benefits are related to diagnosis improvement of airway pathologies, preoperative planning and follow-up. The segmentation issue becomes even more challenging with regard to the high variability of the MSCT image acquisition in clinical practice due to the different CT scanners used and the various protocols (mainly at low dose). This paper develops a generic and automated 3D airway segmentation approach able to deal with a large spectrum of MSCT protocols by exploiting a combined morphological-aggregative methodology. The proposed method was independently assessed by an external group of medical experts in the context of a segmentation challenge, on a database consisting of 20 thorax MSCT datasets. This database included acquisitions from several clinical centers equipped with different CT scanners and using various protocols. The evaluation results show a good performance of the developed approach in terms of airway segments detection accuracy, in the context of highly variable MSCT input data.

1   Introduction

Many approaches dedicated to the segmentation of airways from CT data have been developed in the last decade [1–9], but today there is no independent evaluation of their robustness and accuracy with respect to the variability of the clinical protocols and the CT devices used in clinical practice.

This paper develops an automated and generic method for 3D airway reconstruction from MSCT and assesses it by an independent expert consortium on a shared database (http://image.diku.dk/exact/) specially built-up to match most of the current situations met in clinical routine. The segmentation scheme and the options used for the adaptation to the MSCT protocols are presented in detail in Section 2. The independent evaluation results and an overall discussion are given in Section 3.

2   Method

The approach presented in this paper is an extension to low-dose MSCT acquisitions of the technique developed in [9]. It consists of two main steps, airway candidates selection and distal airway reconstruction, which are discussed in the following. The method is applied to grayscale windowed MSCT data obtained from the original Hounsfield Unit (HU) values using the LUNG window [-1000, 250] HU. During data conversion, the scan orientation is automatically corrected by comparing the surface of the body cross-section on the first/last ordered images in the DICOM sequence. The lungs are detected on a coronal projection (volume rendering) of the DICOM volume by means of morphological operators and the first/last images of the sequence are set-up according to the lungs extent.

2.1   Airway candidates selection

The selection of the airway candidates exploits the *flood size-drain leveling (FSD)*[1] morphological operator which is defined as follows. Let $f : X \subset \Re^3 \to \Re$ denote the 3D image relief, and $g_n : X \to \Re$ a constraint function derived from f by means of an increasing operator:

$$g_n = \min(f \oplus B_n, \ f \oplus \check{B}_n), \tag{1}$$

where B_n denotes an upstream neighborhood of size n, $\check{B}_n$ the symmetric set of B_n with respect to its origin, and $\oplus$ the Minkowski addition. Note that $g(x) \geq f(x), \forall x \in X$. The flood size-drain leveling of f "floods" the f relief up to a "draining" level imposed by the size of the f "basins" (Fig. 1), and can be expressed by means of the *grayscale reconstruction by erosion* [10] operator as:

$$FSD_f^n = \mathcal{R}^\epsilon{}_f(g_n) = \ominus_f^\infty(g_n), \tag{2}$$

where $\ominus_f^\infty(g)$ denotes the geodesic erosion of g within f, of infinite size, and g_n is given by eq. 1.

Let us consider the image f in Fig. 1(a), top row, and its interpretation in terms of topographic relief, bottom row. f is a two-dimensional simulation of a pulmonary field, where the central structure represents the airway tree, and the small-size valleys denote other low-regions in the lung parenchyma. The idea exploited in [9] for airway candidate selection consists of applying the FSD_f^n operator in a multiresolution scheme, first using a small n-value to "flood" small-size "valleys" disconnected from valleys of size larger than n (Fig. 1(b)), then using a n-value equal to the size of the trachea, in order to "flood" the airway region (Fig. 1(c)). Airway candidates result from an adaptive thresholding of the difference between the filtered data (Fig. 1(d)).

Note that, the FSD ability to "flood" a given region in the image depends on two factors: the region topography should be basin-like and its size has to be smaller than the FSD size. In low-dose MSCT data, noise and partial volume effect may induce local intensity reduction at the level of the airway wall,

---

[1] previously introduced as *sup-constrained connection cost* [9]

which in terms of topographic image interpretation is equivalent with a wall interruption (Fig. 2(a)). In this case, the FSD operator will fail to select the region surrounded by the airway wall, as this zone is no more a "basin" in the image relief (Fig. 2(b)). In order to preserve the selection property required, we define an additional constraint related to the size m of the largest accepted interruption in the basin's wall. An extended operator results, the *closing FSD*, given by:

$$C_m FSD_f^n = \mathcal{R}^\epsilon{}_{f \bullet S_m}(g_n), \tag{3}$$

where $f \bullet S_m$ denotes the morphological closing of f by a spherical structuring element of radius m. Note that, a generalization of such operator can be obtained by replacing the morphological closing with any function $h \geq f$. By applying the CSFD operator with a small m-size (usually $m = 1$), the basin selection property is preserved (Fig. 2(c),2(d)).

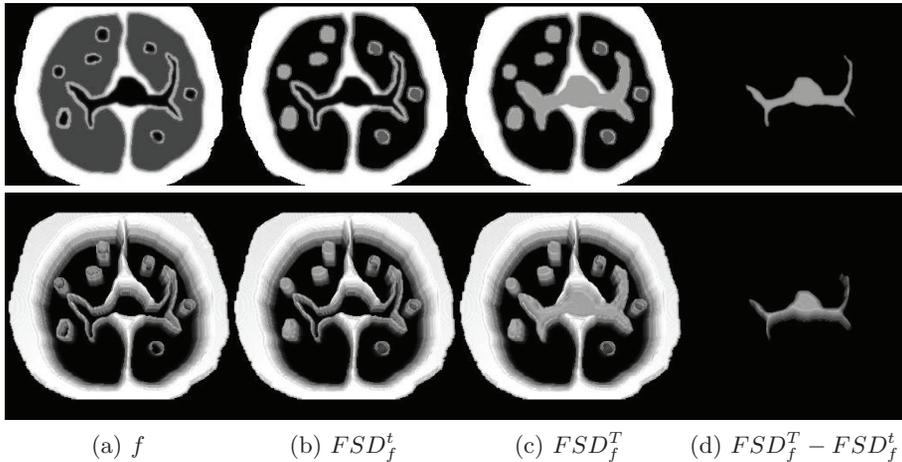(a) f (b) FSD_f^t (c) FSD_f^T (d) $FSD_f^T - FSD_f^t$

Fig. 1. Illustration of the FSD filtering principle used in airway candidates selection in [9].

Note however that, the CT acquisition protocol may impact on the topographic properties of the image relief which describes the airway lumen as "basins" in the lung parenchyma. Consequently, several filters may be applied to the original data (smoothing, median, directional) prior to the candidate selection scheme. Their parameters will be discussed in Section 3. The airway candidates are obtained according to the procedure synthesized in Fig. 3, while Fig. 4 illustrates some intermediate results. First, the trachea cross-section is detected on the first image of the MSCT volume, then the whole trachea is extracted down to the level of the carina (bifurcation into the main bronchi), using a region-growing approach, Fig. 4(a). The maximum size of the trachea cross-section, T, is simultaneously computed. A successive filtering of the MSCT relief f using $C_m FSD_f^n$ is performed as in Fig. 2, first with $n = 3$ for noise suppression,

then using $n = T$ for airway flooding. An adaptive thresholding of the difference $C_{fill}(f) = C_m FSD_f^T - C_m FSD_f^t$ provides a first candidates set for airways, Fig. 4(b). The threshold is automatically computed on the non-zero region of $C_{fill}(f)$ which is spatially connected with the trachea. The threshold value is given by $s = \mu + 2\sigma$, where μ and σ denote respectively the mean and standard deviation estimated for $C_{fill}(f)$ values belonging to the [1, 25] interval. An artifact reduction procedure is applied slice-by-slice and validates each candidate cross-section which has at least 50% contour points adjacent to a dense tissue (bronchus wall). Parts of invalid components (Fig. 4(b), gray) which are upward/downward connected with a valid component are also preserved, Fig. 4(c).
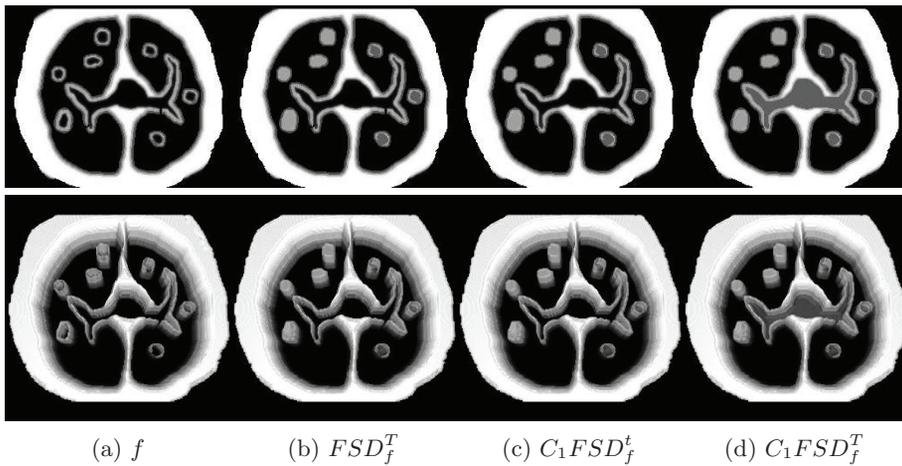

(a) f (b) FSD_f^T (c) $C_1 FSD_f^t$ (d) $C_1 FSD_f^T$

Fig. 2. Illustration of the $C_m FSD$ filtering principle for airway candidates selection.
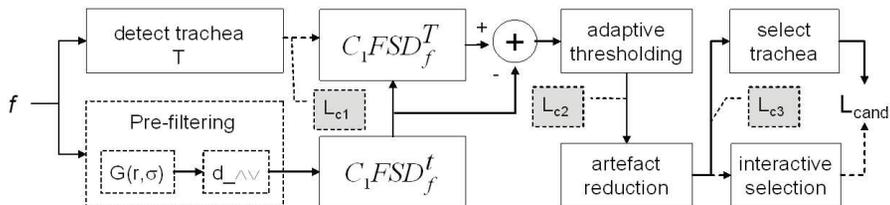

Fig. 3. Airway candidates selection: synoptic scheme.

At this point, the procedure can perform in two modes, automatic or semi-automatic. In the automatic mode, the airway candidates are selected as the only 3D component connected with the trachea, previously detected, Fig. 4(d).

In the semi-automatic mode, the user interactively selects the components to keep.
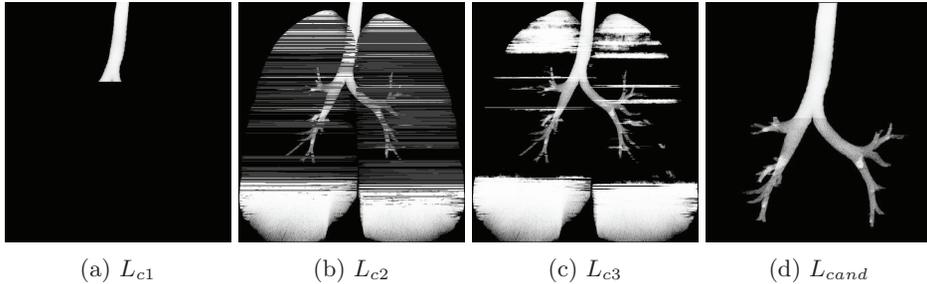

(a) L_{c1} (b) L_{c2} (c) L_{c3} (d) L_{cand}

Fig. 4. Intermediate results of the automatic airway candidate selection procedure of Fig. 3.

Note that, in particular cases where the airway lumen intensity is locally higher than the normal, due to respiratory or metallic artifacts, cardiac motion, mucoid impaction or stenoses, several connected components of airway candidates will be present, and, in this case, an interactive selection mode is recommended.

2.2   Distal airway reconstruction

The reconstruction of distal airways exploits several propagation schemes which are applied iteratively, until the convergence is reached. The propagation starts from the airway candidates which are supposed to be properly located inside the airway lumen, and progressively invests the lung regions. Three conditions have to be met by the new aggregated zones (voxels):

1. either belong to a "tunnel" configuration in terms of tissue density/image intensity, which applies mainly to the reconstruction of small-caliber airways,
2. or belong to a quasi-constant region inside the airway lumen, which applies to the segmentation of medium-caliber bronchi,
3. and avoid or, at least limit, the "leakage" in the lung parenchyma; in this respect, an additional constraint, let us call it "viscosity", can be imposed in the propagation scheme in order to locally stop the growth.

If L_{cand} denotes the airway candidates subset, $\nu \in L_{cand}$ a border point, x a free neighbor of ν (in 26-connectivity), and $f : Y \subset \Re^3 \rightarrow \Re$ the CT image intensity function, the following propagation schemes are defined in order to test the inclusion of x in L_{cand}.

A. Low-resolution tunnel propagation (LRTP)

Generally associated with a low-pass filtering (Gaussian smoothing) of the original CT data f, it requires the acceptance of at least one of the following conditions:
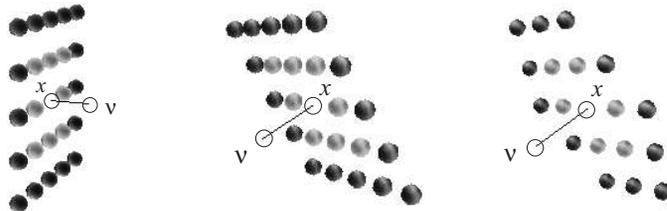
1. Test of tunnel configuration

A local neighborhood of x orthogonal to the propagation direction $\overline{\nu x}$ of first $(\vartheta_{1,\nu}^{\perp}(x))$ and second order $(\vartheta_{2,\nu}^{\perp}(x))$ is used, Fig. 5. The following criteria have to be simultaneously met:

- x is a local minimum of f with respect to the neighborhood $\vartheta_{1,\nu}^{\perp}(x) \cup \vartheta_{2,\nu}^{\perp}(x)$, i.e. $\forall y \in \vartheta_{2,\nu}^{\perp}(x)$, there is no descending path on the f relief restricted to $\vartheta_{1,\nu}^{\perp}(x) \cup \vartheta_{2,\nu}^{\perp}(x)$, leading from x to y.
- if y denotes the mass center of the $\{f(\vartheta_{1,\nu}^{\perp}(x) \cup \vartheta_{2,\nu}^{\perp}(x))\}$ and $d(x,y)$ the Euclidean distance between x and y (in voxel units), then $d(x,y) \leq d_c(x)$, where $d_c(x) = 2$ for "viscous" propagation, otherwise $d_c(x) = \{\sqrt{3}, 2, 3\}$ for x $\{6-, 18-, 26-\}$ connected neighbor of ν.
- if ρ denotes the correlation coefficient computed between the "relief" of $f(\vartheta_{1,\nu}^{\perp}(x) \cup \vartheta_{2,\nu}^{\perp}(x))$ and a bowl-shape, x is added to L_{cand} if either (1) $\rho \geq 0.5$, or (2) $0.2 < \rho < 0.5$ and a f value increase in the $\overline{\nu x}$ direction is checked, $f(x + \overline{\nu x}) > min\{f(\vartheta_{1,\nu}^{\perp}(x))\}$ and $f(x + 2\overline{\nu x}) > min\{f(\vartheta_{2,\nu}^{\perp}(x))\}$.

2. Test of quasi-constant region inside the airway lumen

Such test is performed in a 5-voxel length region in the $\overline{\nu x}$ propagation direction.

- first, to avoid the leakage in the parenchyma, a f value large enough to be considered as airway wall should be found in a cone-shaped neigborhood of x, on each direction $\overline{\nu y}$, $y \in \vartheta_{n,\nu}(x)$ (Fig. 6), within a distance of $T/3$, where T denotes the size of the trachea cross-section (*cf.* §2.1).
- second, considering the directional neighborhoods of x in Fig. 6, the average value of f computed on each of them should satisfy the relation: $E\{f(\vartheta_{n,\nu}(x))\} \leq E\{f(\vartheta_{f,\nu}(x))\}$.
- finally, the f-value oscillation amplitude in the $\overline{\nu x}$ direction should be smaller than a constant $k_o(x) = \{7, 10, 14\}$ for x $\{6-, 18-, 26-\}$ connected neighbor of ν. The f-value oscillation amplitude is computed either along the $\overline{\nu x}$ direction, in normal propagation mode, or within the "far" neighborhood shifted in each point along the $\overline{\nu x}$ segment, $\bigcup_{y \in \overline{\nu x}} \vartheta_{f,\nu}(y)$, in "viscous" propagation mode.

(a) 6-c configuration.   (b) 18-c configuration.   (c) 26-c configuration.

Fig. 5. First and second order neighborhoods of x in the plane orthogonal to $\overline{\nu x}$, $\vartheta_{1,\nu}^{\perp}(x)$ (light grey) and $\vartheta_{2,\nu}^{\perp}(x)$ (dark grey), respectively, according to the $\nu - x$ connectivity.
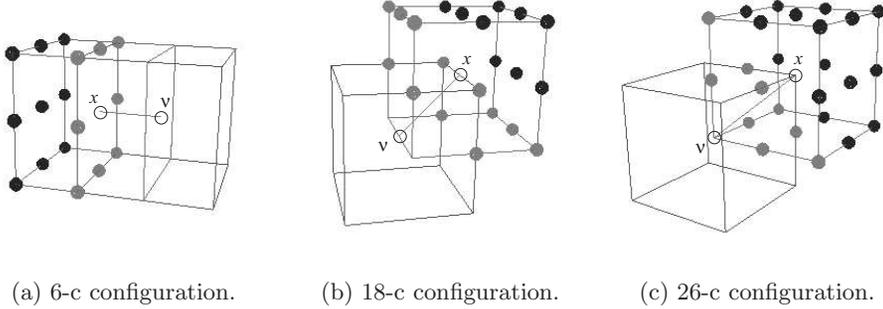
(a) 6-c configuration.   (b) 18-c configuration.   (c) 26-c configuration.

Fig. 6. Directional "near" and "far" neighborhoods of x with respect to its position relative to ν (6-, 18-, 26- connectivity): $\vartheta_{n,\nu}(x)$ (grey) and $\vartheta_{f,\nu}(x)$ (black).
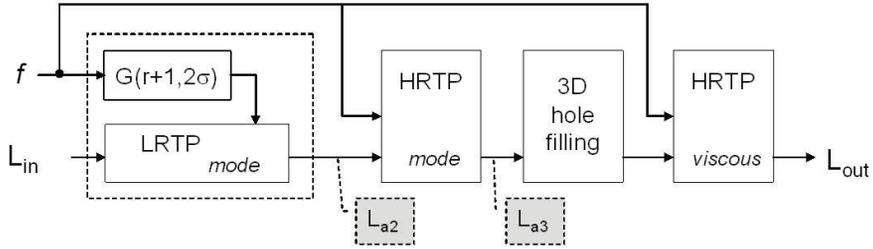
B. High-resolution tunnel propagation (HRTP)

The HRTP scheme includes the same conditions as the LRTP and adds a regularizing one which may facilitate the acceptance of a ν neighbor, x, in the airway lumen set L_{cand}.
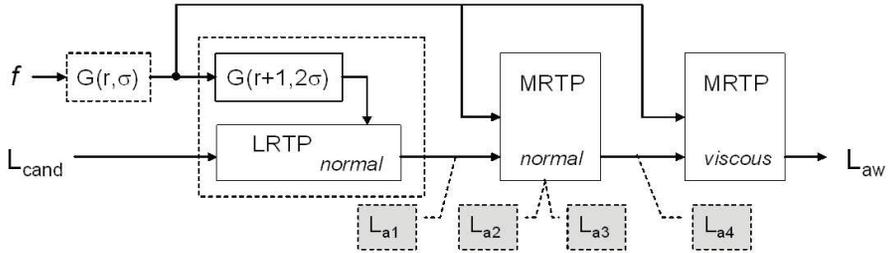
3. Regularization condition

In addition to the first two requirements of the *tunnel configuration test* in LRTP, x has to fulfill a neighborhood occupancy condition: $N_o(x) + \mu_f(x) > N_f(x) + \mu_o(x) + \sigma_o(x) + T_{100}(f(x))$, where $N_o(x)$ and $N_f(x)$ denote respectively the number of occupied and free 26-neighbors of x, $\mu_o(x)$ and $\mu_f(x)$ the average f values computed on $N_o(x)$ and $N_f(x)$, $\sigma_o(x)$ the standard deviation of f on $N_o(x)$, and T_a the thresholding operator, $T_a(u) = \{u, \; if \; u \geq a; \; 0 \; otherwise\}$.

The distal airway reconstruction scheme implemented is summarized in Fig. 7. Note that, as in § 2.1, a prefiltering of the original data f might be needed according to the CT scanning protocol used. These parameters will be discussed in Section 3. A multi-resolution tunnel propagation (MRTP) module is designed as a succession of a LRTP and a HRTP (which can be applied either in normal or "viscous" mode), followed by a 3D hole filling and by a HRTP in "viscous" mode, Fig. 7(a). The distal airway reconstruction starts by reinforcing the airway candidates by means of a LRTP in normal mode, Fig. 7(b). Then, the MRTP scheme is applied successively in normal and "viscous" mode. The intermediate propagation results are illustrated in Fig. 8.

(a) Multi-resolution tunnel propagation (MRTP) scheme.

(b) Distal airways reconstruction.

Fig. 7. Reconstruction of distal airways: synoptic scheme. Note that, if no data pre-filtering is used ($r = 0$), then $\sigma = 0.1$ in the LRTP scheme.

(a) L_{a2} (b) L_{a3} (c) L_{a4} (d) L_{aw}

Fig. 8. Intermediate and final results of the distal airway segmentation procedure of Fig. 7(b).

3   Results and discussion

The developed segmentation approach was assessed in the framework of the EXACT'09 challenge (http://image.diku.dk/exact/) by a group of independent experts[11]. The evaluation database included 20 pairs of anonymized MSCT cases of various pathologies, acquired in different hospital centers using several CT scanners and protocols (Table 1). Half of them represented the training test, for algorithm parameter tune-up, and the other half constituted the testing set.

A ground truth was defined as the union of all valid airway segments from all submitted segmentations, and all submissions were subsequently evaluated with respect to this ground truth.

Table 1. Description of the evaluation dataset, the algorithm parameters used and the recorded running time (test set only). Here, G denotes a Gaussian filter of parameters G(1,0.2).

CASE number	MSCT scanner	Reconstruction kernel	X-ray dose (mAs)	Colli-mation (mm)	z sam-pling (mm)	Prefiltering Fig. 3 / Fig. 7(b)	Running time (min:sec)
1, 21	Siemens	B50f	200	0.6	0.5	G / G	6:07
2, 22	Siemens	B50f	200	0.6	0.6	G / G	14:11
3, 23	Siemens	B50f	200	0.75	0.5	G / G	12:26
4, 24	Toshiba	FC12	10	1.0	0.8		7:33
5, 25	Toshiba	FC10	150	1.0	0.8		7:34
6, 26	Toshiba	FC12	10	1.0	0.8		3:20
7, 27	Toshiba	FC10	150	1.0	0.8		2:45
8, 28	Siemens	B30f	300	1.25	?		3:59
9, 29	Siemens	B50f	300	1.25	?		4:17
10, 30	Philips	D	120	1.0	1.0		2:04
11, 31	Philips	D	120	1.0	1.0		2:23
12, 32	Philips	D	120	1.0	1.0		3:31
13, 33	Siemens	B60f	222	1.0	1.0		5:20
14, 34	Siemens	B60f	321	1.0	0.8		5:23
15, 35	GE	STD	357	0.625	0.625		4:53
16, 36	Philips	C	184	1.0	0.7		6:57
17, 37	Philips	B	64	1.0	0.7		5:46
18, 38	Philips	C	51	1.0	0.7		5:40
19, 39	Siemens	B70f	361	1.0	1.0	G / G	4:29
20, 40	Siemens	B70s	108	1.0	1.0	$G + d^3_{f \wedge \vee}$ / G	3:56

Airway segments were visually assessed on a set of extracted slices from both a reoriented view and a reformatted view with straightened airway centerlines. Each segment was scored as "correct" or "wrong", by at least two observers. The criterion used is whether the extracted airway segment indeed belongs to the airway tree; the exact airway shape and dimensions were not taken into account.

In our case, the only parameter tuning was at the level of prefiltering of the original data (Fig. 3, 7(b)). The filters considered here were: a Gaussian smoothing $G(r, \sigma)$, where r denotes the kernel radius and σ the considered standard deviation, and/or a directional filter $d^n_{f \wedge \vee}(x)$ which returns the minimum value among the maximum values of f computed along each of the 13 main directions, in a length interval [-n, n]. The use of prefiltering is decided during a protocol-learning phase applied only on the training set, and consisting of three runs of the algorithm, first without filtering, second using $G(r, \sigma)$, and third, using $G(r, \sigma)$ and adding $d^n_{f \wedge \vee}(x)$ in the candidate selection scheme (Fig. 3)

only. The parameters providing the best average results are selected according to the CT manufacturer, reconstruction kernel applied and the X-ray dose ($\leq$ or $>$ 200 mAs). According to the protocol database thus obtained, the prefiltering parameters are automatically selected for the cases in the test set. This ensures the automatism of the proposed approach. For the cases where the prefiltering was selected, the parameters are mentioned in Table 1. Note that, in the absence of the Gaussian smoothing, the low-pass filter associated with the LRTP scheme (Fig. 3, 7(b)) has the parameters G(1,0.2). The airway segmentation procedure was run in automatic mode for all 40 cases.

The evaluation results for the test dataset are shown in Table 2. The following measurements were computed by the external evaluation team and used for comparing the submitted results:

Table 2. Evaluation measures for the twenty cases in the test set.

	Branch count	Branch detected (%)	Tree length (cm)	Tree length detected (%)	Leakage count	Leakage volume (mm^3)	False positive rate (%)
CASE21	115	57.8	62.5	56.6	2	1.5	0.02
CASE22	256	66.1	193.1	58.4	34	915.6	3.02
CASE23	247	87.0	217.7	83.7	30	3973.7	11.62
CASE24	130	69.9	101.5	62.4	3	3.7	0.01
CASE25	146	62.4	115.3	45.8	0	0.0	0.00
CASE26	28	35.0	21.5	32.7	4	5.7	0.11
CASE27	83	82.2	60.3	74.4	2	2.7	0.02
CASE28	82	66.7	61.5	56.1	10	566.1	4.56
CASE29	124	67.4	80.1	58.0	11	280.4	2.02
CASE30	118	60.5	81.4	53.2	2	45.8	0.37
CASE31	117	54.7	86.7	49.4	9	280.8	1.32
CASE32	122	52.4	93.4	42.9	10	1336.1	4.97
CASE33	113	67.3	82.3	56.0	3	10.8	0.11
CASE34	282	61.6	201.6	56.4	15	68.1	0.17
CASE35	192	55.8	134.6	43.5	8	659.8	2.54
CASE36	239	65.7	258.2	62.6	13	88.7	0.26
CASE37	104	56.2	82.5	46.4	1	71.7	0.35
CASE38	52	53.1	40.1	60.4	1	0.4	<0.01
CASE39	336	64.6	256.3	62.6	38	1241.8	3.45
CASE40	269	69.2	217.8	56.3	44	1716.4	4.27
Mean	157.8	62.8	122.4	55.9	12.0	563.5	1.96
Std. dev.	85.1	11.0	73.8	11.2	13.5	959.3	2.86
Min	28	35.0	21.5	32.7	0	0.0	0.00
1st quartile	104	55.8	62.5	46.4	2	3.7	0.02
Median	123	63.5	90.0	56.3	9	80.2	0.36
3rd quartile	256	69.2	217.7	62.6	30	1241.8	4.27
Max	336	87.0	258.2	83.7	44	3973.7	11.62

1. Branch count: the number of branches that are detected correctly. A branch is considered detected as long as the length of the centerlines is more

than 1 mm; **2. Branch detected:** the fraction of branches that are detected, with respect to the branches present in the ground truth; **3. Tree length:** the sum of the length of the centerlines of all correctly detected branches; **4. Tree length detected:** the fraction of tree length in the ground truth that is detected correctly; **5. Leakage count:** the number of unconnected groups of "correct" regions that are neighboring with a "wrong" region (indicates how easy/difficult it is to manually separate leakages from the correctly detected branches); **6. Leakage volume:** the volume of regions that are wrongly detected; **7. False positive rate:** the fraction of the volume of regions that are detected wrongly over the volume of all detected regions.

Fig. 9 illustrates some representative results. Fig. 8(d) concerns the case 22. Note that the airway segmentation accuracy strongly depends on the radiation dose, reconstruction kernel, lung inflation volume, and on the type/severity of the pathology. The presence of image artifacts (respiratory, cardiac motion, metallic) has generally a negative impact on the reconstruction result, mainly when the automatic mode is selected, as airway candidates disconnected from the trachea will be lost and might not be retrieved in the propagation phase. When working in semi-automatic mode, higher accuracy may be achieved at the expense of interaction time.
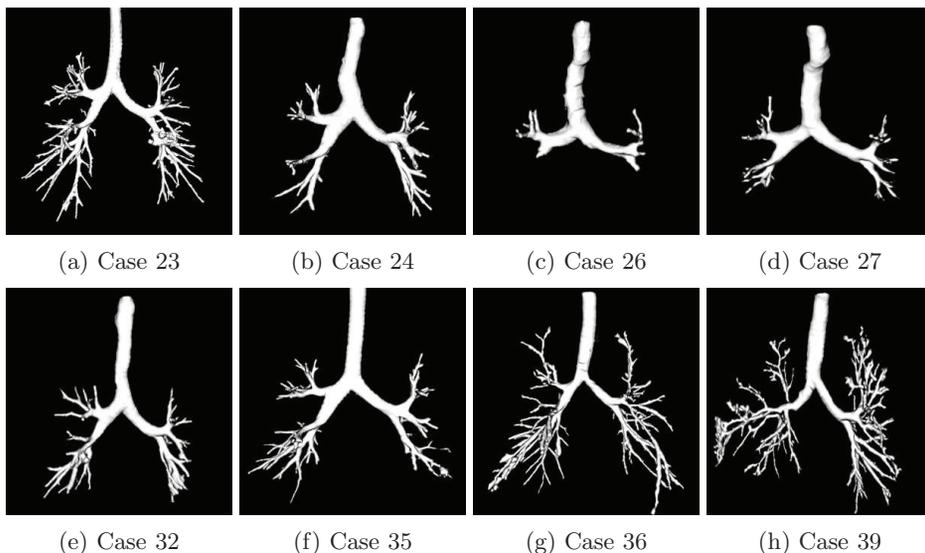

(a) Case 23   (b) Case 24   (c) Case 26   (d) Case 27

(e) Case 32   (f) Case 35   (g) Case 36   (h) Case 39

Fig. 9. Some results of the developed airway segmentation procedure. Illustration using opaque volume rendering.

The algorithm was run on a Dell PowerEdge workstation equipped with Linux Red Hat 5.3 operating system, Intel Xeon CPU 3.4 GHz and 6 GBytes RAM

memory. The execution time recorded for each case of the test set is mentioned in Table 1.

At this stage, we cannot perform a more in-depth analysis of the results obtained with respect to the acquisition protocols used, as some information is missing both in terms of type of pathology and CT protocol parameters that would be able to explain differences shown in airway segmentation.

Concerning the participation to the EXACT'09 airway segmentation challenge, the developed approach reaches a high grading among the fifteen participating teams, as revealed by the average scores published on the EXACT'09 webpage, http://image.diku.dk/exact/results.php. This study stresses out the importance of the MSCT acquisition protocol set-up according to the type of the planned investigation, irrespective to the 3D segmentation approach used.

References

1. Mori, K., Hasegawa, J., Toriwaki, J., Anno, H., Katada, K.: Recognition of Bronchus in Three-Dimensional X-ray CT Images with Applications to Virtualized Bronchoscopy System. In: Proceedings of the 13th International Conference on Pattern Recognition. Volume 3. (1996) 528–532
2. Park, W., Hoffman, E.A., Sonka, M.: Fuzzy logic approach to extraction of intrathoracic airway trees from three-dimensional CT images. In: Proc SPIE. Volume 2710. (1996) 210–219
3. Sonka, M., Park, W., Hoffman, E.A.: Rule-based detection of intrathoracic airway trees. IEEE Transactions on Medical Imaging **15**(3) (1996) 314–326
4. Reinhardt, J.M., D'Souza, N.D., Hoffman, E.A.: Accurate measurement of intrathoracic airways. IEEE transactions on medical imaging **16**(6) (1997) 820 – 827
5. Kiraly, A.P., Higgins, W.E., McLennan, G., Hoffman, E.A., Reinhardt, J.M.: Three-dimensional human airway segmentation methods for clinical virtual bronchoscopy. Academic Radiology **9**(10) (2002) 1153–1168
6. Schlatholter, T., Lorenz, C., Carlsen, I.C., Renisch, S., Deschamps, T.: Simultaneous segmentation and tree reconstruction of the airways for virtual bronchoscopy. In: Proc SPIE. Volume 4684. (2002) 103–113
7. Tschirren, J., Hoffman, E.A., McLennan, G., Sonka, M.: Intrathoracic airway trees: Segmentation and airway morphology analysis from low-dose CT scans. IEEE Transactions on Medical Imaging **24**(12) (December 2005) 1529 – 1539
8. Fetita, C., Prêteux, F., Grenier, P.: 3D reconstruction of the bronchial tree in volumetric CT: application to ct bronchography. Journal of Electronic Imaging **15**(2) (October 2006) 023004–1:17
9. Fetita, C., Prêteux, F., Beigelman-Aubry, C., Grenier, P.: Pulmonary airways: 3D reconstruction from multi-slice CT and clinical investigation. IEEE Transactions on Medical Imaging **23**(11) (November 2004) 1353–1364
10. Vincent, L.: Morphological gray scale reconstruction in image analysis: applications and efficient algorithms. IEEE Trans on Image Processing **2**(2) (1993) 176–201
11. Lo, P., van Ginneken, B., Reinhardt, J., de Bruijne, M.: Extraction of airways from CT (EXACT'09). In: Second International Workshop on Pulmonary Image Analysis. (2009)